Dielectronic Recombination in O⁴⁺ Near the Ionization Threshold

M. S. PINDZOLA AND S. D. LOCH

UDepartment of Physics, Auburn University, Auburn, AL

ABSTRACT: Relativistic perturbation theory calculations are carried out for dielectronic recombination cross sections involving levels in the O^{3+} $1s^22p^23l$ ($l = 0, 1, 2$) configurations. One of the 8 levels in the $1s^22p^23s$ configuration is found to lie above the O^{4+} ionization limit, eight of the 21 levels in the $1s^22p^23p$ configuration are found to lie above the O^{4+} ionization limit, and all 28 levels in the $1s^22p^23d$ configuration are found to lie above the O^{4+} ionization limit. The largest cross sections are found at -2.0 eV for the $1s^22p^23s$ configuration, at 1.2 eV for the $1s^22p^23p$ configuration, and at 1.7 eV for the $1s^22p^23d$ configuration.

1. INTRODUCTION

Resonance states just below the ionization threshold may contribute to dielectronic recombination in astrophysical and laboratory plasmas[1, 2]. Proper inclusion of the below-threshold resonance states may make substantial changes in the thermally averaged rate coefficients.

Recently relativistic perturbation theory calculations were made for the dielectronic recombination cross sections involving the 10 levels in the F^{5+} $1s^22p6p$ configuration[3]. Only one of the 10 levels was found to lie above the F^{6+} ionization limit. In this paper we look at dielectronic recombination in O^{4+} $1s^22s^2$ leading to O^{3+} $1s^22p^23l$ ($l = 0, 1, 2$) resonance states that lie just below and above the ionization threshold.

The rest of the paper is structured as follows: in section 2 we review theory, in section 3 we present results, and in section we give a brief summary. Unless otherwise stated, all quantities are given in atomic units.

2. THEORY

The dielectronic recombination cross section for an N electron ground level with statistical weight g_i combining into an (N+1) electron doubly excited level with statistical weight g_j is given by[4]:

$$\sigma_{i \to j} = \frac{\pi^2}{E_c \Delta E_c} \frac{g_j}{2g_i} A_a(j \to i) B_j \tag{1}$$

where E_c is the energy of the continuum electron and ΔE_c is bin width. The branching ratio for radiative stabilization is given by:

$$B_j = \frac{\sum_n A_r(j \to n)}{\sum_k A_a(j \to k) + \sum_n A_r(j \to n)} \tag{2}$$

where the radiative A_r and autoionization A_a rates are evaluated using lowest order perturbation theory.

For radiative and autoionization rates, the energies and bound state wavefunctions are calculated using a multi-

configuration Dirac-Fock atomic structure code[5]. The continuum state wavefunctions are calculated using a a single-channel radial Dirac equation, where the Dirac local exchange distorting potential is constructed from Dirac-Fock bound radial orbitals.

3. RESULTS

Fully relativistic calculations were carried out for the O^{4+} $1s^22s^2$ subconfiguration leading to an energy of -68.3032 au. Fully relativistic calculations were also carried out for the O^{4+} $(1s^22s^2+1s^22\bar{p}^2+1s^22p^2)$ subconfigurations leading to an energy of -68.3970 au. Energies for the 57 levels associated with the O^{3+} $1s^22\bar{p}^23l(l = 0, 1, 2)$ configurations are based on differences between low-order relativistic calculations for the resonance subconfigurations and fully-relativistic calculations for the O^{4+} $(1s^22s^2+1s^22\bar{p}^2+1s^22p^2)$ subconfiguration.

Low-order relativistic calculations were carried out for the 8 levels of the O^{3+} even-parity subconfigurations: $1s^22\bar{p}^23s$ (1 level), $1s22\bar{p}2p3s$ (4 levels), and $1s^22p^23s$ (3 levels). For added correlation we also included 9 levels from the $1s^22s2p^2$ and $1s^22s^23s$ configurations. Autoionization rates were determined for the decay of the 8 levels of the $1s^22p^23s$ configuration to the 30 levels of the $1s^22s2pkp$ and $1s^22s2pkf$ configurations. Radiative rates were determined for the decay of the 8 levels of the $1s^22p^23s$ configuration to the 5 levels of the $1s^22p^3$ configuration. Energies, autoionization rates, and radiative rates for the 8 levels are presented in Table 1. Dielectronic recombination cross sections for the 8 levels are presented in Figure 1 using $\Delta E_c = 0.04$ eV in Eq.(1). Convoluted dielectronic recombination cross sections for the 8 levels are presented in Figure 2 using a convolution energy of 0.4 eV. We note that the largest convoluted cross section is around -2.0 eV due to the levels $1s^22p^2(0)3s$ 1/2 and $1s^22p^2(2)3s$ 3/2.

Low-order relativistic calculations were carried out for the 21 levels of the O^{3+} odd-parity subconfigurations: $1s^22\bar{p}^23\bar{p}$ (1 level), $1s^22\bar{p}2p3\bar{p}$ (4 levels), $1s^22p23\bar{p}$ (3 levels), $1s^22\bar{p}^23p$ (1 level), $1s^22\bar{p}^2p3p$ (7 levels), and $1s^22p^23p$ (5 levels). For added correlation we also included 4 levels from the $1s^22s^22p$ and $1s^22s^23p$ configurations. Autoionization rates were determined for the decay of the 21 levels of the $1s^22p^23p$ configuration to the 41 levels of the $1s^22s2pks$, $1s^22s2pkd$, and $1s^22s2pkg$ configurations. Radiative rates were determined for the decay of the 21 levels of the $1s^22p^23p$ configuration to the 8 levels of the $1s^22s2p^2$ configuration. Energies, autoionization rates, and radiative rates for the 21 levels are presented in Table 2. Dielectronic recombination cross sections for the 21 levels are presented in Figure 3 using $\Delta E_c = 0.04$ eV in Eq.(1). Convoluted dielectronic recombination cross sections for the 21 levels are presented in Figure 4 using a convolution energy of 0.4 eV. We note that the largest convoluted cross section is around 1.2 eV due to the levels $1s^22\bar{p}2p(2)3p$ 3/2 and $1s^22\bar{p}2p(2)3p$ 5/2.

Low-order relativistic calculations were carried out for the 28 levels of the O^{3+} even-parity subconfigurations: $1s^22\bar{p}^23\bar{d}$ (1 level), $1s^22\bar{p}2p3\bar{d}$ (7 levels), $1s^22p^23\bar{d}$ (5 levels), $1s^22\bar{p}^23d$ (1 level), $1s^22\bar{p}2p3d$ (8 levels), and $1s^22p^23d$ (6 levels). For added correlation we also included 10 levels from the $1s^22s2p^2$ and $1s^22s^23d$ configurations. Autoionization rates were determined for the decay of the 28 levels of the $1s^22p^23d$ configuration to the 53 levels of the $1s^22s2pkp$, $1s^22s2pkf$, and $1s^22s2pkh$ configurations. Radiative rates were determined for the decay of the 28 levels of the $1s^22p^23d$ configuration to the 5 levels of the $1s^22p^3$ configuration. Energies, autoionization rates, and radiative rates for the 28 levels are presented in Table 3. Dielectronic recombination cross sections for the 28 levels are presented in Figure 5 using $\Delta E_c = 0.04$ eV in Eq.(1). Convoluted dielectronic recombination cross sections for the 28 levels are presented in Figure 6 using a convolution energy of 0.4 eV. We note that the largest convoluted cross section is around 1.7 eV due to the levels $1s^22p^2(2)3\bar{d}$ 3/2, $1s^22p^2(2)3\bar{d}$ 5/2, and $1s^22p^2(2)3\bar{d}$ 7/2.

4. SUMMARY

Relativistic perturbation theory has been applied to calculate the dielectronic recombination in O^{4+} above and below the ionization threshold involving levels in the O^{3+} $1s^22p^23s$ (l = 0, 1, 2) configurations. In the future we plan to map out the dielectronic recombination above and below the ionization threshold for the O^{3+} $1s^22s2p4l$ (l = 0, 1, 2, 3) and $1s^22s2p5l$ (l = 0, 1, 2, 3, 4) configurations.

ACKNOWLEDGMENTS

Department of Energy. Computational work was carried out at the National Energy Research Scientific Computing Center (NERSC) in Berkeley, California.

References

[1] Robicheaux F, Loch S D, Pindzola M S, and Ballance C P 2010 Phys. Rev. Letts. 105 233201

[2] Pindzola M S, Loch S D, and Robicheaux F 2011 Phys. Rev. A 83 042705

[3] Pindzola M S and Loch S D 2018 Int. Rev. of Atomic and Molecular Phys. 9b 87

[4] Pindzola M S and Badnell N R 1990 Phys. Rev. A 42 6526

[5] Grant I P 2007 Relativistic Quantum Theory of Atoms and Molecules (Springer, New York)

Table 1. O³⁺ 1s²2p²3s Auger and Radiative Rates

Sub-configuration	J value	Energy	Auger Rate	Radiative Rate
$1s^2 2\bar{p}^2(0)3s$	1/2	-5.50 eV	3.17×10^{14} Hz	2.66×10^9 Hz
$1s^2 2\bar{p}2p(1)3s$	1/2	-5.48 eV	3.22×10^{14} Hz	2.62×10^9 Hz
$1s^2 2\bar{p}2p(1)3s$	3/2	-5.44 eV	1.37×10^{14} Hz	2.56×10^9 Hz
$1s^2 2\bar{p}2p(2)3s$	3/2	-4.18 eV	5.94×10^{15} Hz	5.27×10^9 Hz
$1s^2 2\bar{p}2p(2)3s$	5/2	-4.14 eV	7.39×10^{15} Hz	5.27×10^9 Hz
$1s^2 2p^2(0)3s$	1/2	-1.93 eV	9.63×10^{14} Hz	4.11×10^9 Hz
$1s^2 2p^2(2)3s$	3/2	-1.93 eV	1.76×10^{15} Hz	4.19×10^9 Hz
$1s^2 2p^2(2)3s$	5/2	5.17 eV	1.00×10^{15} Hz	5.60×10^9 Hz

Table 2. O³⁺ 1s²2p²3p Auger and Radiative Rates

Sub-configuration	J value	Energy	Auger Rate	Radiative Rate
$1s^2 2\bar{p}^2(0)3\bar{p}$	1/2	-3.10 eV	2.48×10^{11} Hz	4.93×10^9 Hz
$1s^2 2\bar{p}2p(1)3\bar{p}$	1/2	-2.58 eV	1.45×10^{13} Hz	1.18×10^{10} Hz
$1s^2 2\bar{p}2p(1)3\bar{p}$	3/2	-2.57 eV	1.47×10^{13} Hz	1.18×10^{10} Hz
$1s^2 2\bar{p}2p(2)3\bar{p}$	3/2	-2.54 eV	1.49×10^{13} Hz	1.18×10^{10} Hz
$1s^2 2\bar{p}2p(2)3\bar{p}$	5/2	-2.50 eV	1.52×10^{13} Hz	1.17×10^{10} Hz
$1s^2 2p^2(0)3\bar{p}$	1/2	-2.18 eV	1.16×10^{14} Hz	1.20×10^{10} Hz
$1s^2 2p^2(2)3\bar{p}$	3/2	-2.17 eV	1.15×10^{14} Hz	1.20×10^{10} Hz
$1s^2 2p^2(2)3\bar{p}$	5/2	-2.15 eV	1.14×10^{14} Hz	1.20×10^{10} Hz
$1s^2 2\bar{p}^2(0)3p$	3/2	-1.60 eV	2.09×10^{13} Hz	5.87×10^9 Hz
$1s^2 2\bar{p}2p(1)3p$	1/2	-1.56 eV	2.00×10^{13} Hz	5.89×10^9 Hz
$1s^2 2\bar{p}2p(1)3p$	3/2	-1.37 eV	1.57×10^{11} Hz	1.26×10^{10} Hz
$1s^2 2\bar{p}2p(1)3p$	5/2	-0.91 eV	3.84×10^{14} Hz	5.93×10^9 Hz
$1s^2 2\bar{p}2p(2)3p$	1/2	-0.90 eV	3.81×10^{14} Hz	6.03×10^9 Hz
$1s^2 2\bar{p}2p(2)3p$	3/2	1.16 eV	1.86×10^{13} Hz	9.37×10^9 Hz
$1s^2 2\bar{p}2p(2)3p$	5/2	1.18 eV	2.03×10^{13} Hz	9.31×10^9 Hz
$1s^2 2\bar{p}2p(2)3p$	7/2	1.67 eV	1.06×10^{13} Hz	9.24×10^9 Hz
$1s^2 2p^2(0)3p$	3/2	1.68 eV	1.07×10^{13} Hz	9.26×10^9 Hz
$1s^2 2p^2(2)3p$	1/2	2.36 eV	7.02×10^{14} Hz	8.64×10^9 Hz
$1s^2 2p^2(2)3p$	3/2	2.39 eV	7.20×10^{14} Hz	8.65×10^9 Hz
$1s^2 2p^2(2)3p$	5/2	8.88 eV	1.58×10^{14} Hz	1.01×10^{10} Hz
$1s^2 2p^2(2)3p$	7/2	8.89 eV	1.57×10^{14} Hz	1.01×10^{10} Hz

Table 3. O^{3+} 1s^{2}2p^{2}3d Auger and Radiative Rates

Sub-configuration	J value	Energy	Auger Rate	Radiative Rate
$1s^2 2\bar{p}^2(0)3\bar{d}$	3/2	0.64 eV	2.17×10^{16} Hz	7.11×10^5 Hz
$1s^2 2\bar{p}2p(1)3d$	1/2	0.65 eV	2.09×10^{16} Hz	4.69×10^5 Hz
$1s^2 2\bar{p}2p(1)3\bar{d}$	3/2	0.68 eV	2.07×10^{16} Hz	2.23×10^5 Hz
$1s^2 2\bar{p}2p(1)3\bar{d}$	5/2	0.70 eV	2.08×10^{16} Hz	0.00 Hz
$1s^2 2\bar{p}2p(2)3\bar{d}$	1/2	1.16 eV	1.62×10^{16} Hz	6.92×10^9 Hz
$1s^2 2\bar{p}2p(2)3\bar{d}$	3/2	1.18 eV	1.62×10^{16} Hz	4.18×10^9 Hz
$1s^2 2\bar{p}2p(2)3\bar{d}$	5/2	1.22 eV	1.74×10^{16} Hz	6.77×10^8 Hz
$1s^2 2\bar{p}2p(2)3\bar{d}$	7/2	1.22 eV	1.73×10^{16} Hz	5.10×10^7 Hz
$1s^2 2p^2(0)3d$	3/2	1.22 eV	1.90×10^{16} Hz	3.41×10^9 Hz
$1s^2 2p^2(2)3\bar{d}$	1/2	1.24 eV	1.89×10^{16} Hz	3.53×10^6 Hz
$1s^2 2p^2(2)3\bar{d}$	3/2	1.72 eV	1.59×10^{16} Hz	4.35×10^{10} Hz
$1s^2 2p^2(2)3\bar{d}$	5/2	1.74 eV	1.58×10^{16} Hz	4.39×10^{10} Hz
$1s^2 2p^2(2)3d$	7/2	1.75 eV	1.75×10^{16} Hz	4.42×10^{10} Hz
$1s^2 2\bar{p}^2(0)3d$	5/2	1.83 eV	1.56×10^{16} Hz	7.99×10^9 Hz
$1s^2 2\bar{p}2p(1)3d$	3/2	1.88 eV	1.71×10^{16} Hz	8.16×10^9 Hz
$1s^2 2\bar{p}2p(1)3d$	5/2	3.45 eV	1.06×10^{16} Hz	2.85×10^{10} Hz
$1s^2 2\bar{p}2p(1)3d$	7/2	3.47 eV	9.96×10^{15} Hz	2.90×10^{10} Hz
$1s^2 2\bar{p}2p(2)3d$	1/2	4.51 eV	9.30×10^{15} Hz	9.52×10^6 Hz
$1s^2 2\bar{p}2p(2)3d$	3/2	4.52 eV	9.32×10^{15} Hz	0.00 Hz
$1s^2 2\bar{p}2p(2)3d$	5/2	4.92 eV	9.22×10^{15} Hz	2.56×10^{10} Hz
$1s^2 2\bar{p}2p(2)3d$	7/2	4.93 eV	8.25×10^{15} Hz	2.54×10^{10} Hz
$1s^2 2\bar{p}2p(2)3d$	9/2	4.96 eV	9.91×10^{15} Hz	4.74×10^{10} Hz
$1s^2 2p^2(0)3d$	5/2	4.97 eV	1.01×10^{16} Hz	4.76×10^{10} Hz
$1s^2 2p^2(2)3d$	1/2	5.94 eV	9.00×10^{15} Hz	1.72×10^{10} Hz
$1s^2 2p^2(2)3d$	3/2	6.02 eV	9.70×10^{15} Hz	3.40×10^{10} Hz
$1s^2 2p^2(2)3d$	5/2	6.02 eV	9.71×10^{15} Hz	3.41×10^{10} Hz
$1s^2 2p^2(2)3d$	7/2	12.07 eV	4.45×10^{15} Hz	2.13×10^{10} Hz
$1s^2 2p^2(2)3d$	9/2	12.08 eV	5.33×10^{15} Hz	2.20×10^{10} Hz
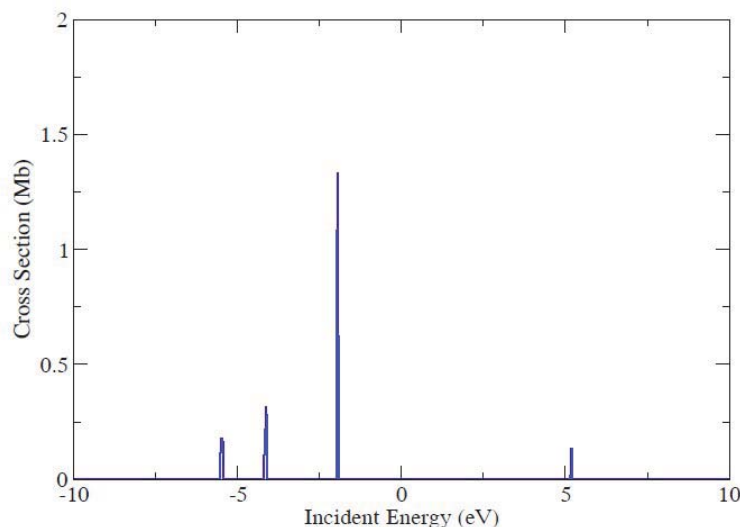
Figure 1. Dielectronic recombination cross sections for O^{4+} 1s^{2}2s^2 via O^{3+} 1s^{2}2p^{3}3s (1.0 Mb = 1.0 × 10^{-18} cm^2).
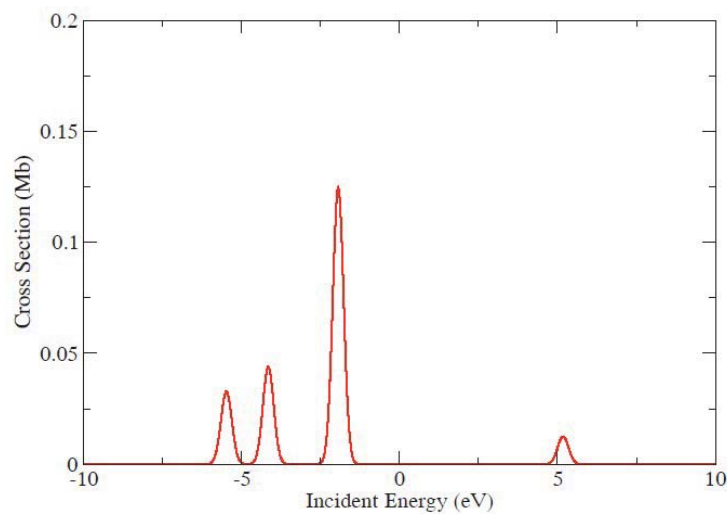
Figure 2. Convoluted dielectronic recombination cross sections for O^{4+} $1s^22s^2$ via O^{3+} $1s^22p^23s$ (1.0 Mb = 1.0 × 10⁻¹⁸ cm²).
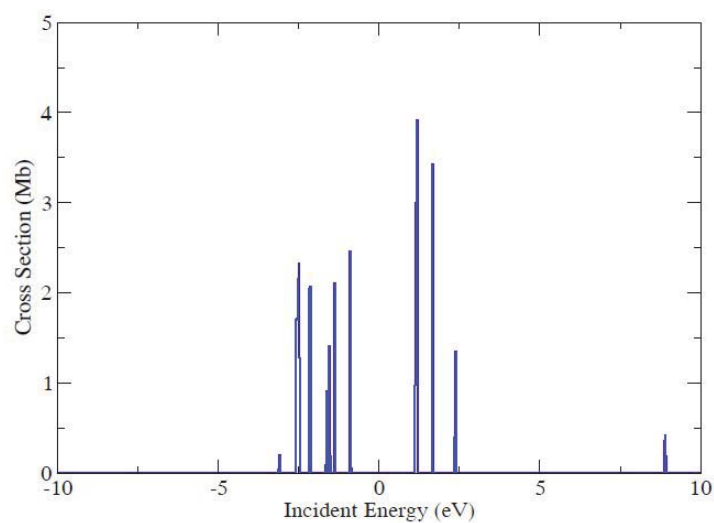
Figure 3. Dielectronic recombination cross sections for O^{4+} $1s^22s^2$ via O^{3+} $1s^22p^23p$ (1.0 Mb = 1.0 × 10⁻¹⁸ cm²).
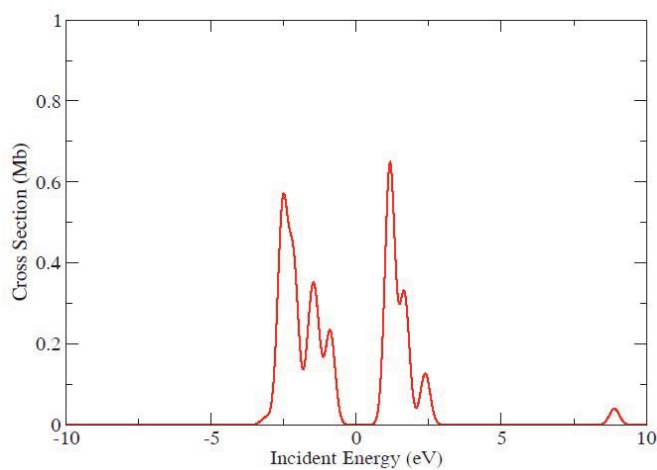
Figure 4. Convoluted dielectronic recombination cross sections for O^{4+} $1s^22s^2$ via O^{3+} $1s_22p^23p$ (1.0 Mb = 1.0 × 10⁻¹⁸ cm²).
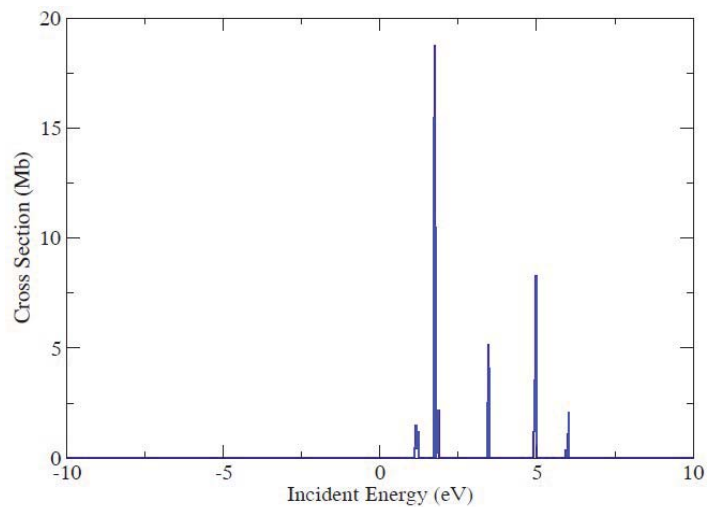
Figure 5. Dielectronic recombination cross sections for O^{4+} 1s^{2}2s^2 via O^{3+} 1s^{2}2p^{3}3d (1.0 Mb = 1.0 × 10^{-18} cm^2).
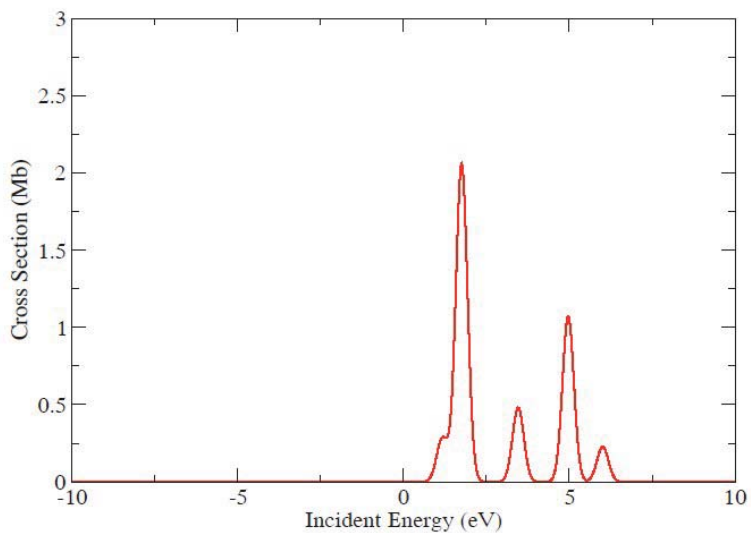
Figure 6. Convoluted dielectronic recombination cross sections for O^{4+} 1s^{2}2s^2 via O^{3+} 1s^{2}2p^{3}3d (1.0 Mb = 1.0 × 10^{-18} cm^2).